
# Model based analysis of the effect of 2-ethylphenol addition to *n*-decane in fluid catalytic cracking over a series of zeolites

Vaios.I. Alexiadis, Moritz Heuchel, Yvonne Traa, Elias Klemm, Nikos Papayannakos, Joris W. Thybaut

PII: S1385-8947(18)31968-5
DOI: https://doi.org/10.1016/j.cej.2018.10.027
Reference: CEJ 20090

To appear in: *Chemical Engineering Journal*

Received Date: 19 June 2018
Revised Date: 16 September 2018
Accepted Date: 4 October 2018

Please cite this article as: Vaios.I. Alexiadis, M. Heuchel, Y. Traa, E. Klemm, N. Papayannakos, J.W. Thybaut, Model based analysis of the effect of 2-ethylphenol addition to *n*-decane in fluid catalytic cracking over a series of zeolites, *Chemical Engineering Journal* (2018), doi: https://doi.org/10.1016/j.cej.2018.10.027

# Model based analysis of the effect of 2-ethylphenol addition to *n*-decane in fluid catalytic cracking over a series of zeolites

Authors :
Vaios.I. Alexiadis[a]
Moritz Heuchel[b]
Yvonne Traa[b]
Elias Klemm[b]
Nikos Papayannakos[c]
Joris W. Thybaut[a,*]

[*] Corresponding authors:
E-mail addresses: Joris.Thybaut@UGent.be (J. W. Thybaut)

[a] *Laboratory for Chemical Technology, Ghent University, Technologiepark 914 B-9052, Ghent, Belgium.*
[b] *Institute of Chemical Technology, University of Stuttgart, Pfaffenwaldring 55, 70569 Stuttgart, Germany*
[c] *School of Chemical Engineering, National Technical University of Athens, Iroon Polytechniou 9 , 15780, Athens, Greeece*

## Abstract

The catalytic cracking of n-decane (C10) purely, representing the conventional gasoil feed, and in admixture with 2-ethylphenol (EP), as a model component for HDO bio-oil, is investigated in a fixed-bed reactor over three faujasites. It was observed that EP induces faster deactivation with time-on-stream (TOS), which was more pronounced when materials with low mesoporous surface area were employed. The gasoline selectivity was also shown to increase more steeply with TOS for an EP containing feed. A 5-lump FCC kinetic model, including selective deactivation functions, was developed and incorporated into a transient reactor model to assess the obtained data and account for the observed effects. With the aid of the model, the above trends were rationalized by an increase in the value of the frequency factors, related to the feed conversion into coke and gasoline. The FCC kinetic model was subsequently integrated into a riser reactor model for pilot level simulations, via the extrapolation of the results obtained based on the transient model for the fixed-bed reactor to the steady-state behavior of a riser reactor. In particular, a unique deactivation factor Φ, reflecting catalyst condition, was introduced in the model for the latter reactor to adequately account for the deactivation functions determined making use of the data acquired in the former. Simulation results demonstrate the significance of the first meters of the riser, as well as the effect of operation parameters, i.e, Φ, EP addition in the feed, inlet catalyst-to-oil ratio, on conversion and selectivities.

Keywords

Fluid catalytic cracking
Zeolites
Kinetic modelling
Deactivation
Oxygenates
Riser

**Nomenclature**

*Latin*

| | |
|---|---|
| $Si$ | *selectivity towards product i, %* |
| $w$ | *weight fraction of n-decane in the feed* |
| Q | *Volumetric flow rate,* $m^3\ s^{-1}$ |
| $F_i$ | *molar flow rate of lump i, mol/s* |
| $TOS$ | *Time on stream, s* |
| $D_{in,r}$ | *inner diameter of fixed-bed reactor, m* |
| $D_{out,th}$ | *Outer diameter of thermowell, m* |
| $k_{o,ij}$ | *Pre-exponential factor for the conversion of lump i to j* |
| $G_i$ | *mass flow rate of lump i, kg/s* |
| $p$ | *pressure, kPa* |
| $T$ | *temperature, K* |
| $E_{a,ij}$ | *Activation energy for the conversion of lump i to lump j, kJ* $mol^{-1}$ |
| $c_p$ | Specific heat capacity, J (kg K)$^{-1}$ |
| $MW_i$ | Molecular weight of lump i, g mol$^{-1}$ |

## 1. Introduction

Fluid Catalytic Cracking (FCC) is one of the most important processes in oil refining and petrochemical industry. It is performed on an acid catalyst containing a zeolite as main active component and converts heavy oil fractions with low commercial value, i.e., atmospheric and vacuum gasoils, into high value products, i.e., gasoline and Liquefied Petroleum Gas (LPG)[1-4]. This process also results in the formation of heavy secondary products on the catalyst, referred to as coke, leading to catalyst activity decay by covering the acid sites and, in a later stage, by blocking the pore network. Apart from its deactivating effect on the catalyst, coke influences also the product selectivity [5, 6]. The FCC industrial unit consists mainly of the riser reactor, where cracking reactions take place, the fluid bed regenerator, used to burn off the coke deposited on the catalyst, and the distillation column(s), for the separation of the products.

The European Union, as a leader of the global environment protection policy, has set the 20-20-20 targets aiming at reducing greenhouse gas emissions by 20% compared to 1990 as a baseline and pursue a share of 20% renewables in the energy sector by 2020 [7]. For the year 2050, a reduction of at least 80% of the greenhouse gas emissions is pursued [8]. These environmental goals necessitate a shift in the energy supply towards biomass and, within the FCC framework, the co-feeding of HydroDeOxynated (HDO) bio-oils, together with the heavy oil feedstocks (co-FCC). HDO bio-oils still contain a considerable amount of oxygen, much lower than the initial 35-40wt% before hydrodeoxygenation, mainly in the form of phenols due to a high activation energy of these molecules.

For a better understanding of the (co-)FCC product selectivities, the hierarchisation degree of the FCC candidate catalysts i.e., the relationship between their micro- and meso-porosity, should be

considered. The mesopores act as a highway for molecular transport and are beneficial for the diffusion of bulky reactants towards and away from the micropores, in which the acid site density is higher and, hence, cracking mainly takes place. For instance, the FAU structure exhibits a large micropore system which is able, together with its high H-transfer ability, to form more aromatics from the phenolic components, as compared to the BEA structure, which exhibits a lower micropore surface area/volume. FAU zeolites also lead to higher isobutane selectivities, whereas BEA zeolites exhibit higher C1-C3 selectivities, due to Haag-Dessau cracking [1,2].

The main challenge in co-FCC process simulation is to relate the feed composition to the product yields for a wide range of operating conditions. This is not straightforward, since the various types of heavy hydrocarbons and oxygenates in the feed react in a different manner and the product slates of the process are the consequence of the complex interplay between reactions such as monomolecular initiation, isomerization, oligomerization or β-scission, and hydride transfer [6, 9]. The complexity of the co-FCC feed and the resulting products spectrum makes it extremely challenging to describe the inherent kinetics at a molecular level. Hence, one is forced to resort to generalities rather than details. An option would be to employ feed model compounds[1, 4, 10-12] and consider the behaviour of groups of components as a unit. Researchers have studied phenols and paraffins as oxygenated and conventional feed model compounds respectively[1, 4] and have grouped similar components into few “lumps” [9, 13-15].

In the present work, the catalytic cracking of n-decane (C10) purely, representing the conventional gasoil feed, and in admixture with 2-ethylphenol (EP), as a model component for HDO bio-oil, is simulated over three faujasites. These materials have been proven to be hydrothermally stable and active under FCC conditions [1, 4] in a continuous flow fixed-bed

reactor configuration. A 5-lump co-FCC kinetic model, including selective deactivation functions, is developed and incorporated into a transient fixed-bed reactor model to assess the reported data [4] and account for the observed effects of EP addition on conversion and selectivities. The co-FCC kinetic model is then integrated into a steady-state riser reactor model, among others by extrapolating the obtained deactivation functions of the transient model to a unique deactivation factor Φ, for these pilot level simulations and predictions.

## 2. Methods and procedures

### 2.1. Experimental

In a previous work twelve commercial faujasites were received from companies and underwent FCC testing with C10 (pure or with 10wt% EP) as feed in a continuous flow fixed-bed quartz reactor under the experimental conditions listed in Table 1 [4]. The obtained evolution of the feed conversion with TOS was reported, while the selectivities towards the various produced compounds, i.e., C1 – C9 hydrocarbons, were compared at iso-conversion, i.e., at a specific TOS [4]. In the current work these compounds are divided into four lumps according to their carbon number, i.e., gasoline, LPG, coke and dry gas, see section 2.2.1., and the feed is considered as one "gas oil" lump. The evolution of gas oil conversion and selectivity towards each lump with TOS over the three most promising materials in terms of activity and stability, i.e., CBV720, CBV712 and 360HUA, is presented and investigated, see section 3.1.

### 2.2. Modelling

#### 2.2.1. Reaction kinetics

A co-FCC kinetic model was developed to assess the experimental data, reported in a previous work [4]. The various reactants and products in this model are divided into five lumps according to their carbon number and boiling point ranges, namely the gas oil (consisting either of pure C10 or of a mixture 10wt% EP in C10), the gasoline (C5-C9), the coke, the LPG (C3-C4) and the dry gas (C1-C2), while individual, selective deactivation functions have been applied, as to enhance the fundamental character and accuracy of the model.

These five groups were incorporated in the reaction network that is depicted in Figure 1. The reactions that are involved in this network are described by eq.1-5 :

$$R_{gas\ oil} = -(k_{12}\phi_{12} + k_{13}\phi_{13} + k_{14}\phi_{14} + k_{15}\phi_{15})c_1^2 \quad (1)$$

$$R_{gasoline} = \upsilon_{12}k_{12}\phi_{12}c_1^2 - (k_{23}\phi_{13} + k_{24}\phi_{24} + k_{25}\phi_{25})c_2 \quad (2)$$

$$R_{LPG} = \upsilon_{13}k_{13}\phi_{13}c_1^2 + \upsilon_{23}k_{23}\phi_{23}c_2 - (k_{34}\phi_{34} + k_{35}\phi_{35})c_3 \quad (3)$$

$$R_{coke} = \upsilon_{14}k_{14}\phi_{14}c_1^2 + \upsilon_{24}k_{24}\phi_{24}c_2 + \upsilon_{34}k_{34}\phi_{34}c_3 \quad (4)$$

$$R_{dry\ gas} = \upsilon_{15}k_{15}\phi_{15}c_1^2 + \upsilon_{25}k_{25}\phi_{25}c_2 + \upsilon_{35}k_{35}\phi_{35}c_3 \quad (5)$$

As can be seen from eq. 1-5, the cracking reactions of gas oil to products were assumed to be of second order, while for the cracking of gasoline and LPG first order kinetics were adopted in line with literature [9]. $R_i$ is the net formation rate of lump i, $k_{ij}$ is the rate coefficient of the reaction of lump i to lump j and $c_i$ is the concentration of lump i. The factor $\upsilon_{ij}$ represents the ratio of the molecular weight of lump i over lump j and is used as stoichiometric coefficient for the reaction of lump i to lump j, to satisfy the global mass balance.

The factor $\phi_{ij}$ represents the catalyst activity of the reaction of lump i to j. The description of activity decay has been modelled, either as an exponential decrease as a function of the time-on-stream (TOS), which is easy to follow despite the fact that TOS is not the appropriate variable to

be employed, or as a function of the amount of coke-on-catalyst. The latter trend although being empirical, uses the variable directly related to activity decay. Hence, the deactivation function

$$\phi_{ij=}\exp(-a_{ij}C_c) \quad (6)$$

has been employed in the current model, where $\alpha_{ij}$ is the deactivation factor and $C_c$ the weight fraction of coke deposited on the catalyst.

In principle an individual deactivation factor should characterize each reaction, yet this will result in a cumbersome regression with an excess of parameters to be estimated. For the sake of simplicity, two cases of selective deactivation were investigated:

*Case 1: reactant oriented deactivation:* The cracking of each reactant (gas oil, gasoline, LPG) is characterized by a constant catalyst deactivation factor, leading to three catalyst deactivation factors $\alpha_{1j}$, $\alpha_{2j}$, $\alpha_{3j}$ and

*Case 2: product oriented deactivation*: The products characterize the catalyst activity towards their production, leading to four catalyst deactivation factors $\alpha_{12}$, $\alpha_{i3}$, $\alpha_{i4}$ and $\alpha_{i5}$.

The first case corresponds with a uniform catalyst site distribution, i.e., the strength of all catalyst active sites is identical and it implies that the blocking of the catalyst pores due to coke formation is the dominant deactivation effect on reactivity. In this case diffusion phenomena are significant and the average molecular size of each reactant plays a dominant role [9].

The product oriented deactivation indicates that different active sites are used for each one of the reactions (eq. 1-5). Furthermore, diffusion phenomena as caging of large hydrocarbon molecules in the catalyst pores by coke deposition, are accounted for leading to selective behavior of the catalyst towards the production of light products [9, 16].

The values for the rate coefficients $k_{ij}$ for the reaction of lump i to lump j are obtained from the Arrhenius equation (apart from $k_{34}$, its value was considered equal to 0 considering that the transformation of LPG to coke does not practically occur [9]) :

$$k_{ij} = k_{0,ij}\exp(-\frac{E_{a,ij}}{RT}) \quad (7)$$

To account for the effect of the feed-gasoil composition (100% C10 or 90%wt C10-EP) on the conversion, the selectivities and the deactivation factors, the specific contribution of EP conversion into aromatics and ethylene, included in the gasoline and dry gas lumps respectively, as well as into coke were considered. The contribution of EP conversion into LPG was considered negligible. Hence, the respective rate coefficients and deactivation factors were further accounted for as :

$$k_{0,1j} = w\, k_{0,1j,C10} + (1-w)k_{0,1j,EP} \quad (8)$$

$$a_{1j} = w\, a_{1j,C10} + (1-w)a_{1j,EP} \quad (9)$$

Where j=2,4,5; w the weight fraction of C10 in the feed; $k_{1j,\ n}$ and $\alpha_{1j,n}$ the individual rate coefficients and deactivation factors respectively which correspond to 100% concentration of n in the feed.

Hydrocarbons form mainly aromatic coke in the micropores of the zeolite, while phenolics can strongly adsorb on the acid sites mainly in the mesopores of the zeolite, due to their large molecular size, forming a phenolic 'pool' by irreversible adsorption and condensation [1,4]. Hence, a more realistic version of the model presented in this work would include selective deactivation functions, such as : $\phi_{ij=}\exp(-w\, a_{ij,C10}C_{c,C10} - (1-w)a_{ij,EP}C_{c,EP})$, where $C_{c,C10}$ and $C_{c,EP}$ represent the weight fraction of coke deposited on the catalyst, originating from C10 and EP respectively. In order not to overparameterize the model, however, the coke origin is not accounted for in our model.

### 2.2.2. Reactor model

#### 2.2.2.1 Transient fixed bed model

The above co-FCC kinetic model was incorporated into an isothermal plug flow fixed-bed reactor model. Transient behavior was considered to account for the effect of TOS on catalyst deactivation and in particular to describe the impact of coke content deposited on the catalyst with TOS on the C10 conversion and product selectivities. The thermowell with outer diameter $D_{out,th}$ inside the reactor was explicitly accounted for in the calculations. Considering that the ratio between the internal diameter $D_{in,r}$ and the catalyst particles diameter is less than 10, plug flow represents an adequate approximation of the reactor hydrodynamics.

The aforementioned kinetic equations eq.1-5 were implemented in the plug flow reactor continuity equation:

$$\frac{\partial F_i}{\partial t} = -\vartheta_z \frac{\partial F_i}{\partial z} + QR_i \qquad (10)$$

where $F_i$ is the molar flow rate of lump i=1,2,3,5; $\vartheta_z$ and Q the linear velocity and the volumetric flow rate of the gas mixture respectively. For i=4, i.e., for coke, convection term was considered negligible. Considering ideal gas mixture, its volumetric flow rate at each point along the reactor axis ,z, was given by the following equation :

$$Q = (RT/p)(F_1 + F_2 + F_3 + F_5) \qquad (11)$$

Where R : gas constant, 8.314 J/(mol K), T : catalyst bed temperature, K and p : reaction pressure, Pa

And the linear velocity was equal to :

$$\vartheta_z = \frac{4Q}{\pi(D_{in,r}^2 - D_{out,th}^2)} \qquad (12)$$

Eq. 10 has the following initial and boundary conditions:

$t=0 \quad F_i=0 \quad , i=1\text{-}5$

$z=0 \quad F_1=F_{1,in}$ and $F_i=0$ for $i=2\text{-}5$

**Model parameters and estimation**

The set of parameters in the constructed co-FCC kinetic model comprises:

- 11 pre-exponential factors : $k_{0,12,C10}$, $k_{0,13}$, $k_{0,14,C10}$, $k_{0,15,C10}$, $k_{0,23}$, $k_{0,24}$, $k_{0,25}$, $k_{0,35}$ , $k_{0,12,EP}$, $k_{0,14,EP}$, $k_{0,15,EP}$
- 8 activation energies : $E_{a,12}$, $E_{a,13}$, $E_{a,14}$, $E_{a,15}$, $E_{a,23}$, $E_{a,24}$, $E_{a,25}$, $E_{a,35}$
- 4 deactivation factors : $\alpha_{1j,C10}$, $\alpha_{2j}$, $\alpha_{3j}$ , $\alpha_{1j,EP}$ (case 1) or
  7 deactivation factors : $\alpha_{12,C10}$ , $\alpha_{i3}$, $\alpha_{i4,C10}$ ,$\alpha_{i5,C10}$, $\alpha_{12,EP}$, $\alpha_{i4,EP}$, $\alpha_{i5,EP}$ (case 2).

The resulting set of equations was solved using *Athena Visual Studio Software for Modeling, Estimation and Optimization 14.2* in which a set of numerical routines has been implemented that allows solving this partial differential equations (PDEs) problem. The code uses the method of lines to solve mixed nonlinear systems of parabolic and first-order PDEs and/or algebraic equations.

**2.2.2.2 Steady-state riser model**

The catalytic cracking reaction occurs, in commercial level, in a riser reactor. Hence, the co-FCC kinetic model was also incorporated into a pilot-level steady state riser reactor model, projecting the kinetics determined by employing the transient fixed bed reactor model, see section 2.2.1. In a riser, vaporized, heavy hydrocarbons crack when contacting the high temperature catalyst coming from the regenerator. The formation of lighter products is invariably accompanied by catalyst deactivation due to coke deposition [3, 9]. The following assumptions for the riser reactor model were made [3, 17]:

i. The riser is modeled employing a 1-dimensional adiabatic reactor model where both axial and radial effective diffusion are neglected, i.e., ideal plug flow is assumed for both gas and catalyst.

ii. Mass and energy balances are written pseudo-homogeneously. No radial and intraparticle gradients are considered. Quasi-steady state is assumed.

iii. The heavy feed enters the bottom of the riser in the gas phase. Ideal gas behaviour.

iv. Thermal equilibrium between the catalyst and the gas phase is achieved instantaneously at the bottom of the riser.

v. The catalyst particles are very small and the vaporized gas carries them at high velocities, hence, the slip factor i.e., the ratio of gas velocity to solid velocity is assumed to be unity.

vi. Catalytic coke is incorporated in the model. Other types of coke are not accounted for. The coke formed on the catalyst surface does not affect gas flow.

**2.2.2.2.1 Mass balance**

The following set of ordinary differential equations has been derived to calculate concentration profiles of the lumps in the gas phase, $x_i$, along the riser position, z:

$$\frac{dG_i}{dz} = \Omega_r \rho_{cat} (1-\varepsilon) R_i MW_i \qquad (13)$$

at z=0, $G_i = G_{i,0}$

with $G_i$ being the mass flow rate of lump i in the gas phase, $kg_i/s$, $\Omega_r$ the riser cross section, $m^2$, $\rho_{cat}$ the density of the catalyst, $kg_{cat}/m^3$, $\varepsilon$ the bed porosity and $R_i$ the net production rate of lump i, $moles_i / (kg_{cat}\ s)$.

The bed porosity, ε, is not constant along the riser but varies according to the following equation:

$$\varepsilon = \frac{\rho_{cat} G_{gas,0}}{\rho_{cat} G_{gas,0} + \rho_{gas} G_{cat,0}} \qquad (14)$$

where $G_{cat,\,0}$ the catalyst mass flow rate at the riser inlet, $kg_{cat}/s$ and $\rho_{gas}$ the gas mixture density. Assuming that slip factor between the gas and the catalyst amounts to unity, the gas mixture density at a specific point along the riser axis, $kg/m^3$, can be obtained from:

$$\rho_{gas} = \frac{P \sum_{i=1}^{5} x_i MW_i}{RT} \qquad (15)$$

where P and T the pressure and temperature at this point of the riser respectively, and $x_i$ the mass fraction of the lump i in the gas mixture.

It is evident from equations 14 and 15 that the bed porosity in principle increases along the riser, since the density of the gas decreases, following the decrease of the molecular weight of the gas mixture. The interstitial porosity increases along the riser , due to the gas expansion, in contrast to the intraparticle porosity, which decreases, due to coke deposition. The latter is considered negligible compared to the former, leading to the overall increase of the bed porosity.

**2.2.2.2.2 Energy balance**

With respect to the derivation of the energy balance equations, it is assumed that thermal equilibrium is instantaneously achieved at the bottom of the riser between the gas and the solid phase due to the large value of the corresponding heat transfer coefficient [3]. This essentially

means that the catalyst and the gas exhibit the same temperature at each point along the riser axis. Accordingly, the riser temperature profile can be obtained from the following energy equation :

$$\frac{1}{\Omega_r}\left(G_{cat,0}c_{p,cat} + G_{gas,0}\, c_{p,gas}\right)\frac{\partial T}{\partial z} = -\rho_{cat}(1-\varepsilon)\left[\sum_{i=1}^{5} R_i\ \Delta H_{f,i}^{0}\right] \quad (16)$$

At z=0, T=$T_{0,}$ where $T_0$ can be calculated from the following equation :

$$G_{cat,0}c_{p,cat}(T_0 - T_{cat}) + G_{gas,0}\, c_{p,gasoil}\left(T_0 - T_{gas}\right) = 0 \quad (17)$$

where $c_{p,cat,}$ $c_{p,gas}$ and $c_{p,gas,0}$ the specific heat capacities of the catalyst, the gas and the gasoil at the riser inlet respectively, J / (kg K), $\Delta H_{f,i}^{0}$ the standard heat of formation for the lump i, J / $kg_{i,}$ $T_{cat}$ and $T_{gas}$ the temperature of the catalyst and the gasoil before they enter the reactor.

**2.2.2.2.3 Kinetic and thermodynamic parameters**

In the riser reactor model, a common deactivation factor Φ was introduced, reflecting the catalyst condition. The concept of a single deactivation factor for all reactions in a riser has been adopted by researchers[18, 19]. In our work, this factor was employed to project the deactivation functions ϕ, calculated for the transient fixed bed model to the steady state riser model (detailed information on this projection procedure is given in the results section 3.2.2).

For the calculation of the reaction enthalpies amongst the lumps, a specific model compound per lump was selected to represent the entire lump. Then the FactSage software (and the NIST database) was employed to generate the reaction heats for the reactions among those compounds at 298K. The reaction enthalpies at the riser temperature, T, were calculated via the following equation :

$$\Delta H_{ij,T} = \Delta H_{ij,298} + \int_{298}^{T} \Delta Cp \, dT \quad (18)$$

where the specific heat capacities are in the form of polynomials, i.e., $Cp = \alpha_1+\alpha_2 T+\alpha_3 T^2+\alpha_4 T^3$, and

$Cp_1 = w\ Cp_{C10} + (1-w)\ Cp_{EP}$, $Cp_2 = Cp_{C5H12}$, $Cp_3 = Cp_{C3H8}$, $Cp_4 = Cp_{graphite}$, $Cp_5 = Cp_{C2H4}$ (19)

## 3. Results and discussion

### 3.1. Experimental results

Figure 2 presents the experimentally observed evolution of gasoil conversion and the selectivity towards each lump with TOS for both gasoil feeds, i.e., pure C10 (left) and in admixture with 10wt% EP (right), for three faujasites, i.e., CBV720, 360HUA and CBV712. These materials were proven to be the most promising, in terms of activity, stability and selectivity towards gasoline and LPG. The (co-)FCC performance of an active, yet unstable material (320HOA), is presented in SI in figure 2 for comparison purposes.

It can be seen that, for both investigated feed compositions, the most active materials are CBV720 and CBV712, followed by 360HUA. CBV720 is slightly more stable than CBV712, with 360HUA being the most unstable zeolite in the low TOS regime (0-10h). All zeolites present high selectivity towards LPG, followed by gasoline and dry gas, with $S_{gasoline}$ increasing with TOS at the expense of $S_{LPG}$, and $S_{dry\ gas}$, phenomenon less pronounced in the case of 360HUA.

By comparing the figures pertaining to pure C10(left) and combined C10-EP(right) feed, it can be concluded that the addition of the oxygenated bio-feed, even at a percentage as low as 10wt%, induces a steeper deactivation of the materials. The relatively smoother deactivation of CBV720

faujasite, compared to the other two materials, when EP is co-fed, can be attributed mainly to its large mesopore area, which can accommodate larger amount of coke[4]. Furthermore, it is deduced from Figure 2 that the increase of gasoline selectivity and the decrease of LPG selectivity with TOS follow a sharper trend in the presence of EP. This can be assigned to the increased formation of aromatics and naphthalenes with EP presence in the feed [4]. The dry gas selectivity either decreases smoother, as in the case of CBV720, or even increases with TOS as in the case of 360HUA catalyst, when 10wt% EP is co-fed, mostly due to the increased production rate of ethylene [4].

## 3.2. Modeling results

### 3.2.1. Transient fixed-bed model validation/regression

In the first instance, the model was assessed describing the experimental data, with pure C10 as feed, produced over each catalyst. For the regression of these data all the model parameters, except the activation energies, were initially allowed to be adjusted. It was found that when the reactant oriented deactivation case was adopted, the model was not able to capture quantitatively and qualitatively the observed feed conversion and selectivity trends. The different effect that time-on-stream has on each product-lump of the scheme was described more accurately when product oriented catalyst deactivation was considered. The calculation results depicted in Figure 2(left) were produced adopting the latter deactivation case and estimating the $\alpha_{12,C10}$ $\alpha_{i3}$, $\alpha_{i4,C10}$ ,$\alpha_{i5,C10}$ deactivation factors, along with the $k_{0,12,C10}$, $k_{0,13}$, $k_{0,14,C10}$ and $k_{0,5,C10}$ pre-exponential factors. Their values are shown in Table 2. The table also presents the values of the remaining pre-exponential factors that were fixed during preliminary simulations and those of the activation energies that were fixed at literature reported values, which were estimated via regression of the lumped model to experimental data, acquired in a conventional FCC pilot plant [9]. In the case

of, e.g., the unstable 320 HOA sample, the model was capable of qualitatively simulating the activity and selectivity trends in line with the observed ones, yet the abrupt behaviour of the conversion in particular, could not be reproduced, see SI Figure 1. A potential explanation is situated in the high activity of this material, due to its high Bronsted acidity, leading to initial conversions of 100% and non-intrinsic kinetics.

The binary correlation coefficient quantifies the extent of association (correlation) of two variables in a single measure ranging from -1 to +1, where -1, +1 and 0 indicate a perfect negative association, a perfect positive association and no association at all, respectively. The maximum absolute value among the binary correlation coefficients amounted to 0.87 and occurred between the pre-exponential factor for the conversion of C10 to coke, $k_{0,14,C10}$ and the respective deactivation factor $\alpha_{i4,C10}$. Such a value allows concluding that there is no significant correlation between the adjustable parameters. The high F value for the global significance of the regression, amounting to 907, illustrates the model's capability of adapting itself to the experimental data.

As can be seen in Table 2, the high activity of CBV720 and CBV712 zeolites for pure C10 feed, see Fig.2(left), can be rationalized by the high values of the pre-exponential factors related to conversion of C10 to gasoline, LPG and dry gas, i.e., $k_{0,12,C10}$ , $k_{0,13,C10}$ and $k_{0,15,C10}$, that these materials exhibit, and mainly the last one. Their high value for $k_{0,15,C10,}$ compared to 360HUA, can be assigned to the higher acidity of these two materials [4]. The relatively high values of $k_{0,14,C10}$ and $\alpha_{i4,c10}$ pertaining to the catalyst 360HUA, imply high coke production which is further suppressed by the deposition of coke itself and account for the steep drop in its activity in the low TOS regime, followed by a smooth drop at higher TOS, see Figure 2 (left). This could be also assigned to the lower number of acid sites this material exhibits [4], rendering its

deactivation rate more sensitive to coke formation.The slightly higher stability of CBV720 compared to CBV712 can also be assigned to the higher $\alpha_{i4,c10}$ that the former catalyst exhibits, since they both present the same $k_{0,14,C10}$.

The relatively high selectivity towards LPG, followed by gasoline and dry gas, that all materials present, see Figure 2(left), is captured by the model mainly through the high $k_{0,13}/k_{0,12,C10}$ ratio and the high activation energy of the reactions leading to dry gas formation, see Table 2. The increase of gasoline selectivity with TOS at the expense of LPG and dry gas selectivity is rationalized by the low value of $\alpha_{i2,c10,}$ compared to $\alpha_{i3}$ and $\alpha_{i5,c10}$, which imply less pronounced suppression of gasoline formation, compared to LPG and dry gas, due to the deposited coke. In the case of 360 HUA, the similar deactivation factors $\alpha_{i2,c10,}$ $\alpha_{i3}$ and $\alpha_{i5,c10}$ it presents, see Table 2, account for the limited effect of coke, and hence TOS, on the product selectivities, see Figure 2(left).

The model was then employed to describe the experimental data produced with the combined feed over each catalyst and Figure 2(right) presents the comparison of the simulated performances to the respective experimental values as a function of TOS. It can be seen that the model describes adequately the effect of the EP co-feeding on the gasoil conversion as well as the selectivity towards gasoline, LPG and dry gas, under the investigated conditions. For the simulation of the above experimental data, the product oriented catalyst deactivation case was adopted, in agreement with the case of the pure C10 feed.

The model parameters that are shown in Table 2 were fixed at the values therein presented, while the pre-exponential factors and activation energies which correspond to pure EP as FCC feed, i.e., $k_{0,12,EP,}$ $k_{0,14,EP}$, $k_{0,15,EP}$ and $\alpha_{12,EP,}$ $\alpha_{14,EP,}$ $\alpha_{15,EP}$ respectively, were allowed to adjust. Their estimated values are presented in Table 3.

From the Tables 2 and 3, it can be seen that $k_{o,14,EP}$ , related to the reaction rate of gasoil into coke, presents higher values than $k_{o,14,C10}$ for all three investigated materials. The formation of the phenolic coke originating from EP takes place to a large extent in the mesopores of the material at a higher rate than that of the aromatic coke, originating from C10, which occurs mainly in the micropores [4]. Hence, the global pre-exponential factor $k_{o,14}$ (via eq.8) increases, see Table 4, accounting for increased cocking rate and the observed steeper deactivation of the investigated materials with TOS in the presence of EP in the FCC feed, see Figure 2(left and right). This phenomenon is more pronounced in the case of 360 HUA material, see Figure 2(left and right), and can be rationalized by the steeper increase of $k_{o,14}$ (compare Table 2 and Table 4), originating from the higher $k_{o,14,EP}$ it presents, see Table 3.

Similarly, $k_{o,12,EP}$ and $k_{o,15,EP}$ , describing the reaction rate of gasoil into gasoline and dry gas respectively, are higher than $k_{o,12,C10}$ and $k_{o,15,C10}$ for all the investigated materials, while the corresponding deactivation factors $a_{12,EP}$ and $a_{15,EP}$ are lower than $a_{12,C10}$ and $a_{15,C10.}$ Hence, the resulting values for the global pre-exponential factors $k_{o,12}$ and $k_{o,15}$ (eq.8) increase and for the global deactivation factors $a_{12}$ and $a_{15}$ decrease (eq.9) with the co-feeding of EP, see Table 4, finding that accounts for the sharp trend of gasoline increase and the smoother decrease or slight increase of dry gas with TOS.

As an alternative to the selected reaction orders in our model, first order kinetics for the C10 feed conversion, given its gasoline range type nature, and second order kinetics for the gasoline conversion have been evaluated. Simulation results (see SI Figure 2) exhibited no considerable improvement of the agreement between calculated and experimental points, compared to the initial assumption, i.e., second order for C10 cracking and first order for gasoline cracking. Even

more strongly, a slight deterioration of the agreement with respect to the feed lump conversion (C10) is observed when its conversion is assumed to be of first order kinetics.

### 3.2.2. Steady-state riser model simulations

#### 3.2.2.1 Determination of kinetic and thermodynamic parameters

The values for the preexponential factors that were estimated during the regression of the fixed bed experimental data were employed in the riser reactor model. The activation energies that were retrieved via the fixed bed reactor modeling were also kept constant in the riser model at their previous values. After a thorough literature survey, it was found that the employed values for the activation energies lie within the range of the literature reported values [9, 13, 14, 20-22].

The compounds with the most elevated concentrations in each lump during the various (co-)FCC experiments were selected to represent the entire lump, i.e., pentane (followed by pentene) for gasoline, propane (followed by propene and butane) for LPG, ethylene (followed by methane) for dry gas, while elemental carbon was selected to represent coke [4]. The reactions as well as the correspondingly calculated enthalpies are presented in Table 5. An extensive literature investigation, performed thereafter, allowed verifying that the calculated values lie within the range of reaction heats reported for the specific reactions among these lumps [13, 14, 21, 23-26]. Hence, they were further employed in the pilot scale riser model.

#### 3.2.2.2 Determination of the unique, common deactivation factor

Figure 3 presents the deactivation functions, related to the decay of the activity of the various reactions among the considered lumps, calculated in the case of CBV720 zeolite with pure C10 and C10 – EP mixture as feed. As seen in Figure 3, $\varphi_{12}$ and $\varphi_{14}$ are the less TOS dependent deactivation functions, irrespective of the feed composition, due to the relative low value of the

corresponding deactivation factors (see Table 2), followed by $\varphi_{13}$ and $\varphi_{15}$.The presence of EP induces faster decay for the activity of all the reactions, e.g., the catalyst activity of reaction of gasoil into gasoline, $\phi_{12}$, drops down to the values of 0.8 and 0.5 at TOS=10h and 20h respectively, while in the case of the combined feed the corresponding TOS are 8h and 15 h. The value of Φ was chosen to be equal to 1, 0,8 and 0,5, representing fresh catalyst, mixture of fresh and regenerated catalyst, and regenerated catalyst respectively. The value of Φ was chosen to correspond to the less TOS dependent deactivation function, $\phi_{12}$, at a specific TOS, i.e., 0, 10 and 20h, and $\phi_{i3}$, $\phi_{i4}$, $\phi_{i5}$ were substituted by their ratio to $\phi_{12}$ at this specific TOS.

Therefore the equations 1-5 of the transient fixed bed reactor model were substituted by equations 20-24 in the steady state riser model :

$$R_{gas\ oil} = -\Phi(k_{12} + k_{13}\phi_{13}/\phi_{12} + k_{14}\phi_{14}/\phi_{12} + k_{15}\phi_{15}/\phi_{12})c_1^2 \quad (20)$$

$$R_{gasoline} = \Phi(v_{12}k_{12}c_1^2 - (k_{23}\phi_{13}/\phi_{12} + k_{24}\phi_{24}/\phi_{12} + k_{25}\phi_{25}/\phi_{12}))c_2 \quad (21)$$

$$R_{LPG} = \Phi(v_{13}k_{13}\phi_{13}/\phi_{12}c_1^2 + v_{23}k_{23}\phi_{23}/\phi_{12}c_2 - (k_{34}\phi_{34}/\phi_{12} + k_{35}\phi_{35}/\phi_{12}))c_3 \quad (22)$$

$$R_{coke} = \Phi(v_{14}k_{14}\phi_{14}/\phi_{12}c_1^2 + v_{24}k_{24}\phi_{24}/\phi_{12}c_2 + v_{34}k_{34}\phi_{34}/\phi_{12}c_3) \quad (23)$$

$$R_{dry\ gas} = \Phi(v_{15}k_{15}\phi_{15}/\phi_{12}c_1^2 + v_{25}k_{25}\phi_{25}/\phi_{12}c_2 + v_{35}k_{35}\phi_{35}/\phi_{12}c_3) \quad (24)$$

For example, in the case of CBV720 zeolite with pure C10 as feed, when Φ=1, then $\phi_{i3}/\phi_{i2}$=1, $\phi_{i4}/\phi_{i2}$=1 and $\phi_{i5}/\phi_{12}$=1.For Φ=0,8, the ratios are determined as $\phi_{i3}/\phi_{i2}$=0.91, $\phi_{i4}/\phi_{i2}$=0.96, $\phi_{i5}/\phi_{12}$=0.88 and for Φ=0.5, the corresponding ratios are 0.75, 0.90 and 0.67.

**3.2.2.3 Simulation results**

The simulation and discussion of a reference case, showcasing the effect and physical meaning of Φ, is performed first. Special attention is paid to feed conversion, cracked product selectivities, temperature and bed porosity profiles through the riser. Riser dimensions, operating conditions and catalyst properties used for this base case simulation are presented in Table 6. Further, an analysis of the effect of the EP addition in the feed and the catalyst-to-oil ratio on the (co-) FCC performance is presented.

The evolution of feed, i.e., pure C10, conversion and product selectivities, as well as that of temperature and bed porosity along the riser position for three different values of Φ at the reference conditions, summarized in Table 6, is presented in Fig. 4. Simulation results show that, within the first 3-4 meters of the riser, C10 conversion typically exceeds 60% and more than 70%wt of the gasoline and LPG observed at the outlet has already been formed, see Figure 4. The initial and steep temperature decrease is due to the vigorous endothermic reactions [3]. The bed porosity increases along the riser axis, following the feed conversion trend.

As can be seen from Figure 4, the decrease of the value of Φ results in a smoother increase of conversion and a smoother decrease of temperature, due to lower cracking rates. A slight increase of gasoline selectivity at the expense of dry gas and LPG selectivity can be also observed from Figure 4. This trend is attributed to the decrease of the values for the $\phi_{i3}/\phi_{i2}$ and $\phi_{i5}/\phi_{i2}$ ratios with the decrease of Φ, see section 3.2.2.2. The effect of Φ in the bed porosity evolution along the riser axis under these operating conditions is negligible, see Figure 4.

The simulated effect of the EP introduction to the FCC feed on the evolution of conversion, product selectivities, temperature and bed porosity along the riser axis is depicted in Figure 5 for Φ=0.8, i.e. for an industrially relevant case of a mixture of regenerated and fresh catalyst. As can be observed in Figure 5, there is virtually no effect on the conversion, selectivities, temperature

and bed porosity profiles along the riser. This is because the lower CBV720 catalyst activity of the reactions of gasoil to gasoline, coke and dry gas (compare $\phi_{12}$, $\phi_{14}$ and $\phi_{15}$, Figure3(left and right)) compensate for the higher pre-exponential factors related to these reactions over this material, when EP is co-fed, see Tables 2,3 and 4.

From Figure 6 it can be seen that the evolution of feed conversion and the product selectivities are rather sensitive to variations of the cat-to-oil ratio. Increasing the cat-to-oil ratio from 2 to 6 $kg_{cat}/kg_{feed}$ results in steeper increase of conversion along the riser axis and 10% more feed conversion, i.e., from 83.5 to 92%, at the riser outlet, due mainly to the increase of the available cracking sites. Another reason could be the increase of the catalyst inlet temperature, which is accounted by the model via the equation 17. Hence, cracking reactions start at a higher temperature resulting in higher feed conversions to cracked products.

The increase of cat-to-oil ratio from 2 to 6 results also in the increase mainly of $S_{dry\ gas}$, by 260%, and $S_{LPG}$ at a lesser extent, by 4%, at the expense of gasoline selectivity, which decreases by 40%. This can be assigned to overcracking of gasoline to dry gas with the increase of cat-to-oil ratio under the investigated range of operating conditions [3]. This phenomenon becomes less pronounced by increasing further the cat-to-oil ratio to 10, see Figure 6.

As mentioned before, the values of the reaction heats, utilised in our model, were determined via FactSage software and not retrieved from literature. To further explore the accuracy of the model, it was tested employing values for reaction enthalpies reported by several groups [13,14,21,23-26]. The simulation results, presented in SI Figure 3a and 3b, deviate negligibly from those acquired by utilising the determined values (SI Figure 3c).

## 4. Conclusions

A (co-)FCC kinetic model was constructed considering five lumps, i.e. gasoil, gasoline, liquefied petroleum gas, coke and dry gas. The model includes also individual selective deactivation functions, which relate the catalyst coke content to the activity of the catalyst for each reaction among the lumps. This model was implemented into a PFR reactor model with transient behavior and was validated against literature data, after their treatment, acquired under identical operating conditions with pure C10 and with combined feed C10-10wt% EP over each of 3 investigated catalysts. It was shown that when product-oriented selective catalyst deactivation was considered, the model simulated correctly the activity and selectivity trends observed over all materials under the investigated operating conditions. It was observed experimentally that EP induces faster deactivation with TOS, which was more pronounced when materials with low mesoporous surface area were employed. The gasoline selectivity was also shown to increase more steeply with TOS for an EP containing feed. With the aid of a 5-lump FCC kinetic model, the above trends were rationalized by an increase in the value of the frequency factors, related to the feed conversion into coke and gasoline. The FCC lumped kinetic model was then implemented successfully into a steady-state riser reactor model, where thermal equilibrium is considered between catalyst and gas. The information contained in the deactivation functions was translated into a unique deactivation factor. Simulation results demonstrated the significance of the first meters of the riser, with respect to feed conversion and temperature profiles. The resulting model also accounted for the effect of operation parameters, i.e., catalyst condition, inlet cat/oil ratio and EP addition in the feed, on performance. It was found that the decrease of $\Phi$ leads to lower conversion and higher $S_{gasoline}$ , the increase of cat-to-oil ratio induces higher conversion and overcracking of gasoline, while the addition of EP had virtually no effect on the riser performance under the investigated conditions. An experimental

verification of these simulation trends will ascertain these conclusions drawn from the kinetic analysis, rendering the developed kinetic model a useful tool for the prediction of the impact of hydrotreatment severity on co-FCC reactor performances.

## Acknowledgements :

This paper reports work undertaken in the context of the project "FASTCARD : FAST industriliazation by CAtalysts Research and Development", supported by the European Commission in the 7th Framework Programme (GA n°604277). JWT acknowledges the ERC for the PoC grant SERENiTi (GA n°825783).

## 5. References

[1] M. Heuchel, F. Reinhardt, N. Merdanoglu, E. Klemm, Y. Traa, Co-catalytic cracking of n-decane and 2-ethylphenol over a variety of deactivated zeolites for the conversion of fossil- and bio-based feeds in Co-FCC, Micropor Mesopor Mat, 254 (2017) 59-68.
[2] R. Quintana-Solorzano, J.W. Thybaut, G.B. Marin, A single-event microkinetic analysis of the catalytic cracking of (cyclo)alkanes on an equilibrium catalyst in the absence of coke formation, Chem Eng Sci, 62 (2007) 5033-5038.
[3] R. Quintana-Solorzano, J.W. Thybaut, P. Galtier, G.B. Marin, Simulation of an industrial riser for catalytic cracking in the presence of coking using Single-Event MicroKinetics, Catal Today, 150 (2010) 319-331.
[4] M. Heuchel, C. Dorr, R. Boldushevskii, S. Lang, E. Klemm, Y. Traa, The influence of porosity and active sites of zeolites Y and beta on the co-cracking of n-decane and 2-ethylphenol, Appl Catal a-Gen, 553 (2018) 91-106.
[5] G. Jimenez-Garcia, R. Quintana-Solorzano, R. Aguilar-Lopez, R. Maya-Yescas, Modelling Catalyst Deactivation by External Coke Deposition during Fluid Catalytic Cracking, Int J Chem React Eng, 8 (2010).
[6] R. Quintana-Solorzano, J.W. Thybaut, P. Galtier, G.B. Marin, Single-event microkinetics for coke formation during the catalytic cracking of (cyclo)alkane/1-octene mixtures, Catal Today, 127 (2007) 17-30.
[7] https://ec.europa.eu/clima/policies/strategies/2020_en, (Accessed : 09/04/2018).
[8] https://ec.europa.eu/clima/policies/strategies/2050_en, (Accessed : 09/04/2018).
[9] G.M. Bollas, A.A. Lappas, D.K. Iatridis, I.A. Vasalos, Five-lump kinetic model with selective catalyst deactivation for the prediction of the product selectivity in the fluid catalytic cracking process, Catal Today, 127 (2007) 31-43.

[10] A.T. To, D.E. Resasco, Hydride transfer between a phenolic surface pool and reactant paraffins in the catalytic cracking of m-cresol/hexanes mixtures over an HY zeolite, Journal of Catalysis, 329 (2015) 57-68.
[11] I. Graca, J.M. Lopes, M.F. Ribeiro, F.R. Ribeiro, H.S. Cerqueira, M.B.B. de Almeida, Catalytic cracking in the presence of guaiacol, Appl Catal B-Environ, 101 (2011) 613-621.
[12] I. Graca, F.R. Ribeiro, H.S. Cerqueira, Y.L. Lam, M.B.B. de Almeida, Catalytic cracking of mixtures of model bio-oil compounds and gasoil, Appl Catal B-Environ, 90 (2009) 556-563.
[13] P.K. Dasila, Choudhurym I., Saraf, D., Chopra, S., Dalai, A., Parametric Sensitivity Studies in a Commercial FCC Unit, Advances in Chemical Engineering and Science, 2 (2012) 136-149.
[14] P.K. Dasila, I.R. Choudhury, S. Singh, S. Rajagopal, S.J. Chopra, D.N. Saraf, Simulation of an Industrial Fluid Catalytic Cracking Riser Reactor Using a Novel 10-Lump Kinetic Model and Some Parametric Sensitivity Studies, Ind Eng Chem Res, 53 (2014) 19660-19670.
[15] D.V. Naik, V. Karthik, V. Kumar, B. Prasad, M.O. Garg, Kinetic modeling for catalytic cracking of pyrolysis oils with VGO in a FCC unit, Chem Eng Sci, 170 (2017) 790-798.
[16] R. Quintana-Solorzano, J.W. Thybaut, G.B. Marin, Catalytic cracking and coking of (cyclo)alkane/1-octene mixtures on an equilibrium catalyst, Appl Catal a-Gen, 314 (2006) 184-199.
[17] I.C. P.K. Dasila, D. Saraf, S. Chopra, A. Dalai, Parametric Sensitivity Studies in a Commercial FCC unit, Advances in Chemical Engineering and Science, 2 (2012) 136-149.
[18] C. Derouin, D. Nevicato, M. Forissier, G. Wild, J.R. Bernard, Hydrodynamics of riser units and their impact on FCC operation, Ind Eng Chem Res, 36 (1997) 4504-4515.
[19] C.I.C. Pinheiro, J.L. Fernandes, L. Domingues, A.J.S. Chambel, I. Graca, N.M.C. Oliveira, H.S. Cerqueira, F.R. Ribeiro, Fluid Catalytic Cracking (FCC) Process Modeling, Simulation, and Control, Ind Eng Chem Res, 51 (2012) 1-29.
[20] J. Ancheyta, F. Lopez-Isunza, E. Aguilar-Rodriguez, 5-Lump kinetic model for gas oil catalytic cracking, Appl Catal a-Gen, 177 (1999) 227-235.
[21] R.B. Kasat, D. Kunzru, D.N. Saraf, S.K. Gupta, Multiobjective optimization of industrial FCC units using elitist nondominated sorting genetic algorithm, Ind Eng Chem Res, 41 (2002) 4765-4776.
[22] K. Xiong, C.X. Lu, Z.F. Wang, X.H. Gao, Quantitative correlations of cracking performance with physiochemical properties of FCC catalysts by a novel lump kinetic modelling method, Fuel, 161 (2015) 113-119.
[23] Y.M. John, R. Patel, I.M. Mujtaba, Modelling and simulation of an industrial riser in fluid catalytic cracking process, Comput Chem Eng, 106 (2017) 730-743.
[24] I.S. Han, C.B. Chung, Dynamic modeling and simulation of a fluidized catalytic cracking process. Part II: Property estimation and simulation, Chem Eng Sci, 56 (2001) 1973-1990.
[25] S.V. Nayak, S.L. Joshi, V.V. Ranade, Modeling of vaporization and cracking of liquid oil injected in a gas-solid riser, Chem Eng Sci, 60 (2005) 6049-6066.

[26] A. Arbel, I.H. Rinard, R. Shinnar, Dynamics and Control of Fluidized Catalytic Crackers .2. Multiple Steady-States and Instabilities, Ind Eng Chem Res, 34 (1995) 3014-3026.

**Figure 1.** Schematic of the proposed 5-lump FCC model [9]

**Figure 2.** Evolution of gasoil, i.e. pure C10 (left) or 10wt%EP-90wt%C10 (right) conversion and product selectivities with TOS over three faujasites. Yellow: C10 conversion; blue: selectivity to gasoline; red: selectivity to lpg; grey: selectivity to dry gas. Symbols : experimental points; lines: calculated results by employing the model described in sections 2.2.1 and 2.2.2.1. Operating conditions listed in Table 1.

**Figure 3**. Deactivation functions , calculated for the CBV720 zeolite with either pure C10 or combined C10-EP feed, with the transient fixed-bed model described in section 2.2.2.1. Operating conditions listed in Table 1.

**Figure 4.** Evolution of C10 conversion and product selectivities (top), temperature and bed porosity (bottom) along the riser reactor axis over CBV720 zeolite for three different Φ values. Operating conditions : Listed in Table 6. Yellow: C10 conversion; blue: selectivity to gasoline; red: selectivity to LPG; grey: selectivity to dry gas; black : selectivity to coke; purple : temperature; green : bed porosity**.** Simulation results were obtained employing the riser reactor model described in sections 2.2.2.2, 3.2.2.1 and 3.2.2.2.

**Figure 5.** Evolution of feed, i.e., pure C10 or mixture C10-10wt%EP, conversion and product selectivities (top), temperature and bed porosity (bottom) along the riser reactor axis over CBV720 zeolite. Operating conditions : Listed in table 6, Φ=0.8. Yellow: gasoil conversion; blue: selectivity to gasoline; red: selectivity to LPG; grey: selectivity to dry gas; black : selectivity to coke; purple : temperature; green : bed porosity. Simulation results were obtained employing the riser model described in sections 2.2.2.2, 3.2.2.1 and 3.2.2.2.

**Figure 6.** Evolution of C10-10wt%EP mixture conversion and product selectivities along the riser reactor axis over CBV720 zeolite for six catalyst-to-oil ($kg_{cat}/kg_{oil}$) ratios. Operating conditions : Listed in Table 6, Φ=0.8. Yellow: gasoil conversion; blue: selectivity to gasoline; red: selectivity to LPG; grey: selectivity to dry gas; black : selectivity to coke. Simulation results were obtained employing the riser model described in sections 2.2.2.2, 3.2.2.1 and 3.2.2.2.

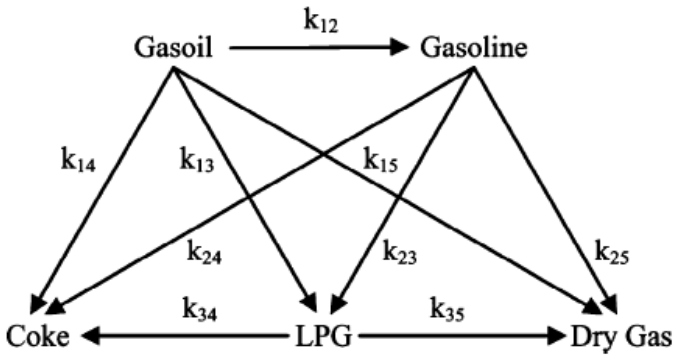


**Figure 1**

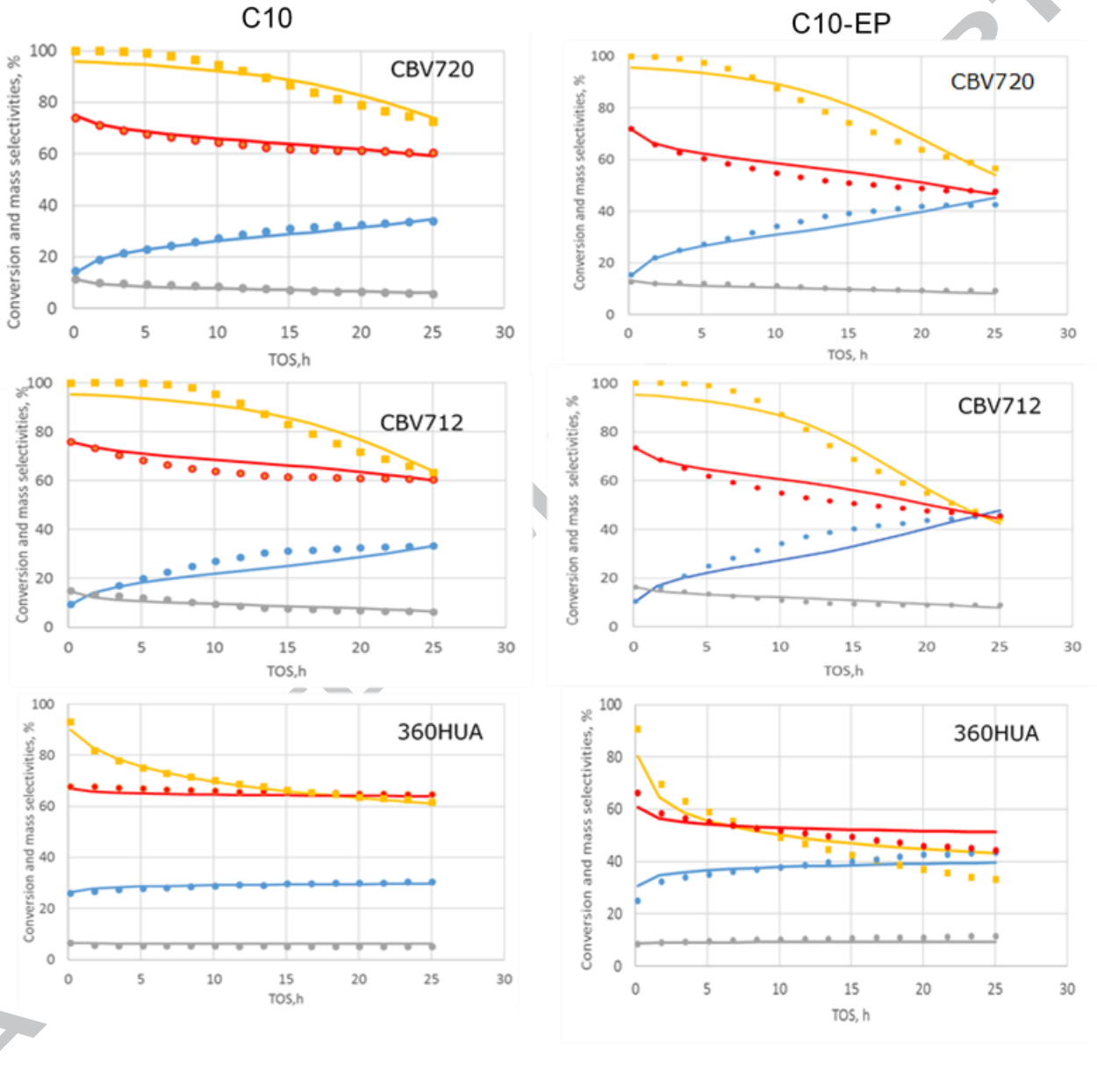


**Figure 2**

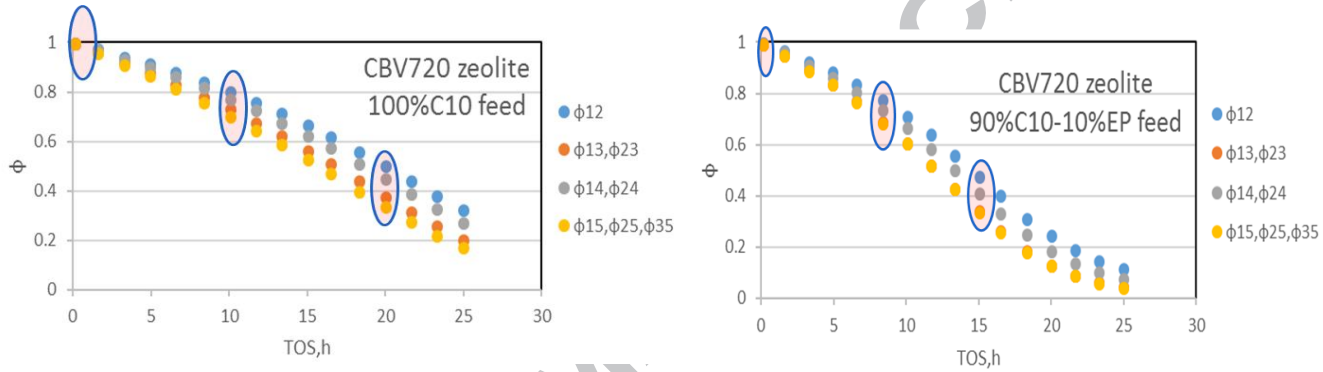


**Figure 3**

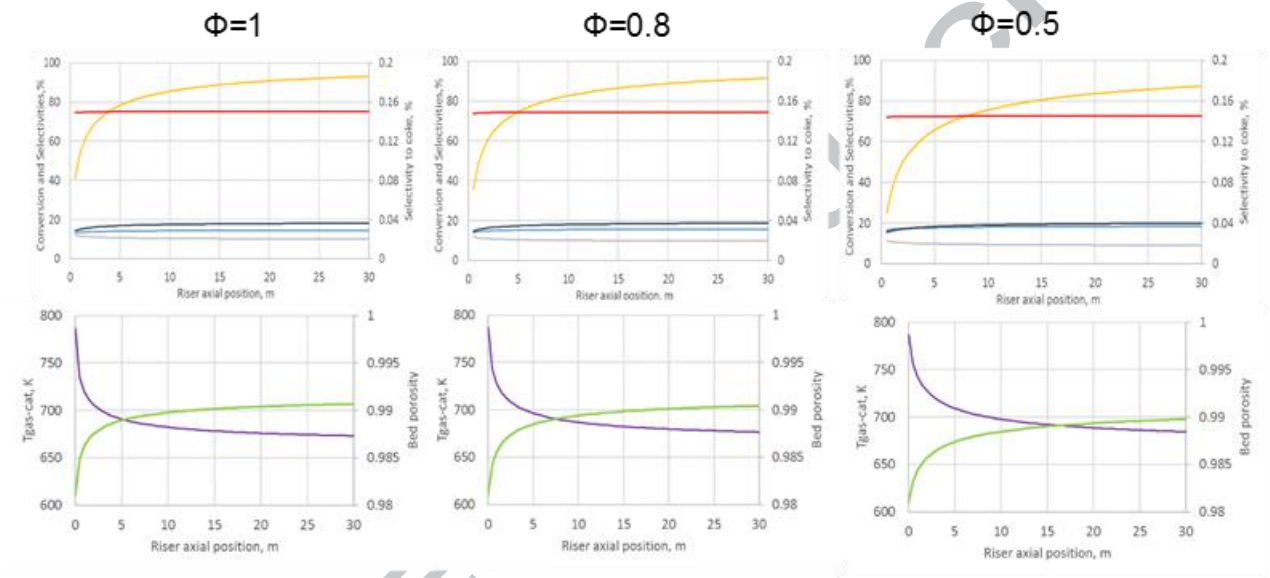
Φ=1
Φ=0.8
Φ=0.5
Conversion and Selectivities, %
Selectivity to coke, %
Riser axial position, m
Tgas-cat, K
Bed porosity

**Figure 4**

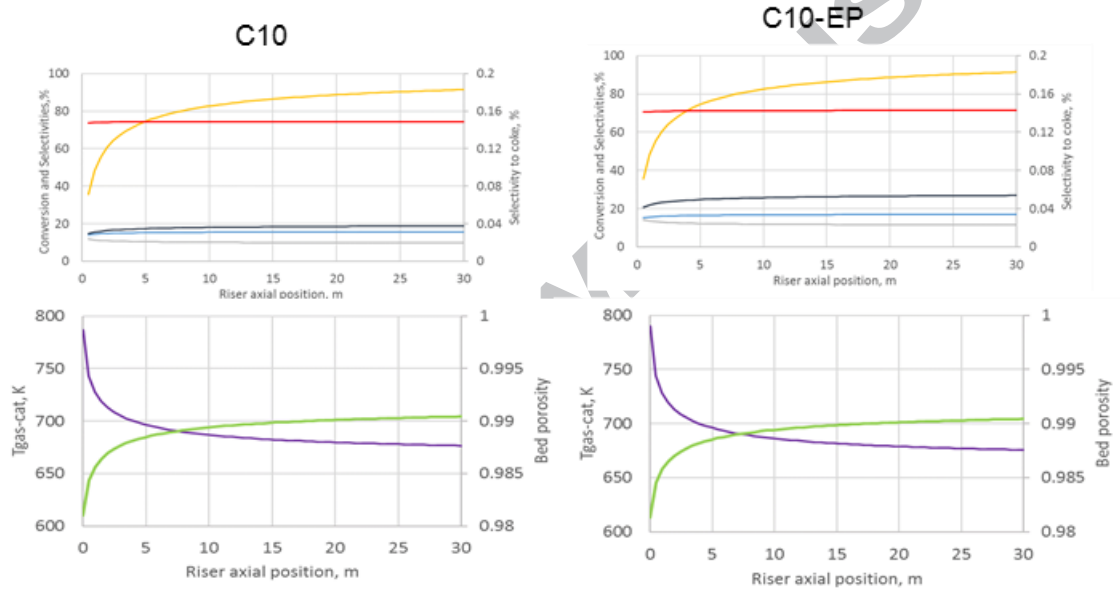


**Figure 5**

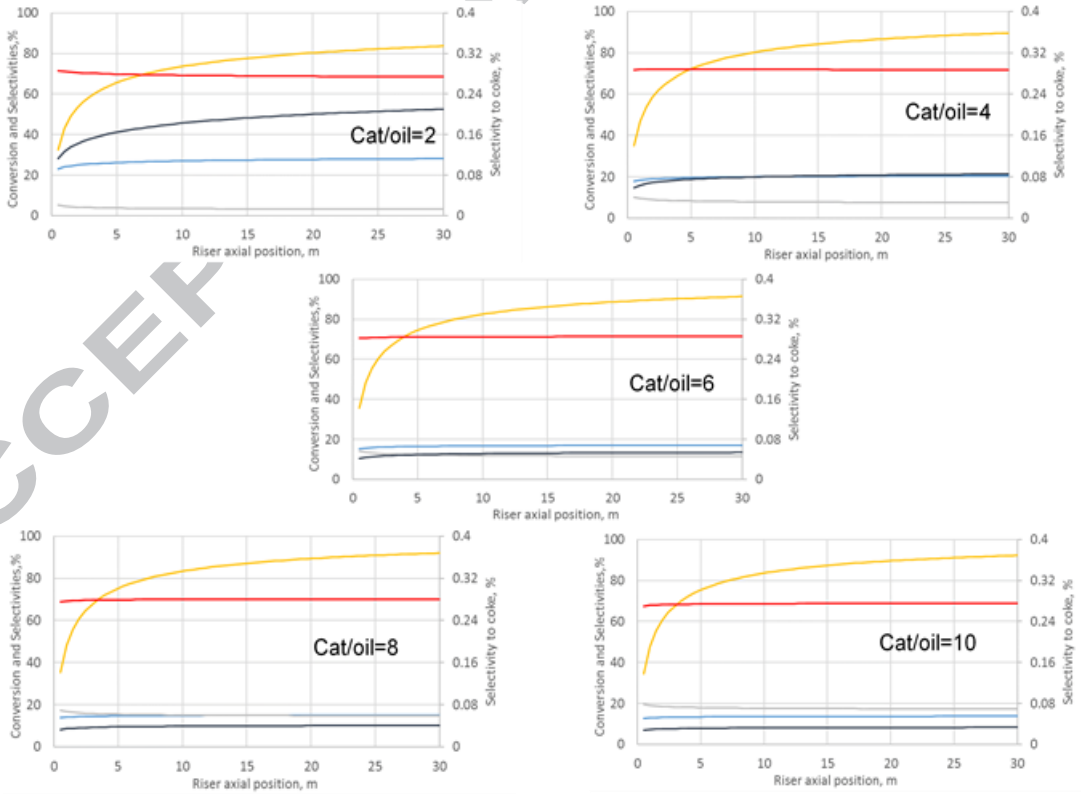

**Figure 6**

**Table 1.** Operating conditions during the (co-)FCC testing over the investigated catalysts [4]

| | | |
|---|---|---|
| Pressure | Pa | 101325 |
| Bed temperature | K | 753 |
| $Feed_{,in}$ | g $s^{-1}$ | 1.4 $10^{-5}$ |
| Catalyst loading | g | 6 $10^{-1}$ |
| TOS | h | 25 |
| Bed length | m | 2.2 $10^{-2}$ |
| $D_{in,r}$ | m | 9.7 $10^{-3}$ |
| $D_{out,th}$ | m | 4 $10^{-3}$ |

**Table 2**. Estimates for the pre-exponential and the deactivation factors pertaining to the investigated catalysts for FCC of pure C10*

| | 360HUA | CBV712 | CBV720 |
|---|---|---|---|
| $k_{0,12,C10}$ | 2.45±0.04 E+5 | 2.58±0.11 E+5 | 3.92±0.1 E+5 |
| $k_{0,13}$ | 4.09±0.13 E+6 | 1.42±0.08 E+7 | 1.44±0.05 E+7 |
| $k_{0,14,C10}$ | 2.76±0.05 E+2 | 5.58±0.04 E+1 | 5.56±0.02 E+1 |
| $k_{0,15,C10}$ | 5.56±0.23 E+7 | 4.05±0.18 E+8 | 3.16±0.13 E+8 |
| $\alpha_{12,C10}$ | 1.01±0.005 E+4 | 5.33±0.16 E+3 | 5.69±0.11 E+3 |
| $\alpha_{i3}$ | 1.07±0.19 E+4 | 8.15±0.24 E+3 | 8.04±0.17 E+3 |
| $\alpha_{i4,C10}$ | 2.67±0.09 E+4 | 6.35±0.1 E+3 | 6.59±0.06E+3 |
| $\alpha_{i5,C10}$ | 1.06±0.11 E+4 | 9.40±0.15 E+3 | 8.99±0.24 E+3 |

Fixed parameters : $k_{0,23}$=32.82, $k_{0,24}$=1.2E-5, $k_{0,25}$=31.41, $k_{0,35}$=31.82
$E_{a,12}$=29.75, $E_{a,13}$=41.59, $E_{a,14}$=12.51, $E_{a,15}$=72.55, $E_{a,23}$=69.83, $E_{a,24}$=13.1, $E_{a,25}$=112.72, $E_{a,35}$=98.49

*Pre-exponential factors given in $g_{cat}$ $wtfract_{coke/cat}$ $mol^{-1}$ $s^{-1}$ for $k_{0,12,C10}$, $k_{0,12,EP}$, $k_{0,13}$, $k_{0,14,C10}$, $k_{0,14,EP}$, $k_{0,15,C10}$, $k_{0,15,EP}$ and in $wtfract_{coke/cat}$ $s^{-1}$ for $k_{0,23}$, $k_{0,24}$, $k_{0,25}$, $k_{0,35}$. Activation energies are given in kJ/mol.

**Table 3.** Estimates for the pre-exponential and the deactivation factors, corresponding to pure EP feed, for the co-FCC of C10-EP mixture*

| | | | | |
|---|---|---|---|---|
| $k_{0,12,EP}$ | 3.12±0.14 E+5 | | 5.34±0.38 E+5 | 8.01±0.29 E+5 |
| $k_{0,14,EP}$ | 2.36±0.07 E+4 | | 3.23±0.06 E+2 | 3.26±0.08 E+2 |
| $k_{0,15,EP}$ | 2.67±0.33 E+8 | | 9.57±0.11 E+8 | 8.90±0.07E+8 |
| $\alpha_{i2,EP}$ | 5.99±0.2 E+2 | | 3.23±0.23E+3 | 4.01±0.1 E+3 |
| $\alpha_{i4,EP}$ | 7.79±0.15 E+3 | | 6.41±0.11 E+3 | 6.65±0.06 E+3 |
| $\alpha_{i5,EP}$ | 1.20±0.03 E+2 | | 4.19±0.07 E+2 | 3.59±0.06 E+2 |

All other parameters fixed at the values presented in Table 2.

*Pre-exponential factors given in $g_{cat}$ $wtfract_{coke/cat}$ $l^{-1}$ $s^{-1}$ for $k_{0,12,C10}$, $k_{0,12,EP}$, $k_{0,13}$, $k_{0,14,C10}$, $k_{0,14,EP}$, $k_{0,15,C10}$, $k_{0,15,EP}$ and in $wtfract_{coke/cat}$ $s^{-1}$ for $k_{0,23}$, $k_{0,24}$, $k_{0,25}$, $k_{0,35}$. Activation energies are given in Kj/mol.

**Table 4.** Calculated values (from eq.8 and eq.9) for the global pre-exponential and deactivation factors corresponding to the combined C10-EP feed*

| | |
|---|---|
| Reaction enthalpies, J/mol (298K) | Calculations (FactSage, NIST) |

*Pre-exponential factors given in $g_{cat}$ $wtfract_{coke/cat}$ $mol^{-1}$ $s^{-1}$ for $k_{0,12}$, $k_{0,14}$, $k_{0,15}$

| | |
|---|---|
| ΔH12 | 78200 ( $C_{10}H_{22}$ -> $C_5H_{12}$ + $C_5H_{10}$ ) |
| ΔH13 | 162500 ( $C_{10}H_{22}$ -> $C_3H_8$ + $C_3H_6$ + $C_4H_8$ ) |
| ΔH14 | 245500 ( $C_{10}H_{22}$ -> 10C + 11$H_2$ ) |
| ΔH15 | 406700 ( $C_{10}H_{22}$ -> 4.5$C_2H_4$ + $CH_4$ ) |
| ΔH23 | 41700 ( $C_5H_{12}$ -> 0.5 $C_3H_8$ + 0.5 $C_3H_6$ + 0.5$C_4H_{10}$ ) |
| ΔH24 | 146400 ( $C_5H_{12}$ -> 5C + 6$H_2$ ) |
| ΔH25 | 176500 ( $C_5H_{12}$ -> 2$C_2H_4$ + $CH_4$ ) |
| ΔH35 | 81400 ( $C_3H_8$ -> $C_2H_4$ + $CH_4$ ) |

**Table 5.** Calculated reaction enthalpies used in the pilot riser reactor model

**Table 6.** Riser dimensions, operating conditions and catalyst properties employed in the simulations [3]

| | | |
|---|---|---|
| Riser length | m | 30 |
| Riser internal diameter | m | 0.94 |
| Gasoil mass flow rate | kg/s | 52.6 |
| Cat-to-oil ratio | | 6 |
| Gas feed temperature | K | 519 |
| Catalyst temperature | K | 1003 |

| | | |
|---|---|---|
| Riser total pressure | Pa | 193 |
| Catalyst density | kg $m^{-3}$ | 1300 |
| Catalyst specific heat capacity | J $(kg\ K)^{-1}$ | 1003 |

Highlights

- 2-Ethylphenol in the feed induces steeper deactivation and gasoline selectivity increases
- Steeper deactivation is attributed to higher frequency factor for coke production
- Cracking to gasoline proceeds with higher frequency factor
- Projection of deactivation functions from transient fixed-bed to steady state riser model
- Increase of cat-to-oil ratio induces higher feed conversion and overcracking of gasoline